



1 **Gasoline direct injection vehicles exceed port fuel injection ones in both primary aerosol emission and**
2 **secondary aerosol formation**

3 Zhuofei Du¹, Min Hu^{1,3*}, Jianfei Peng^{1†}, Wenbin Zhang², Jing Zheng¹, Fangting Gu¹, Yanhong Qin¹, Yudong Yang¹,
4 Mengren Li¹, Yusheng Wu¹, Min Shao¹, Shijin Shuai²

5 1. State Key Joint Laboratory of Environmental Simulation and Pollution Control, College of Environmental
6 Sciences and Engineering, Peking University, Beijing 100871, China

7 2. State Key Laboratory of Automotive Safety and Energy, Department of Automotive Engineering, Tsinghua
8 University, Beijing 100084, China

9 3. Beijing Innovation Center for Engineering Sciences and Advanced Technology, Peking University, Beijing
10 100871, China

11 † Now at Department of Atmospheric Sciences, Texas A&M University, College Station, TX 77843, US

12

13 *Corresponding author: Min Hu, minhu@pku.edu.cn

14

15

16 **Abstract**

17 Gasoline vehicles greatly contribute importantly to urban particulate matter (PM) pollution. Gasoline direct
18 injection (GDI) engines, known as their higher fuel efficiency than that of port fuel injection (PFI) engines, have
19 been increasingly employed in new gasoline vehicles. However, the impact of this trend on air quality is still poorly
20 understood. Here, we investigated both primary emissions and secondary organic aerosol (SOA) formation from
21 GDI and PFI vehicles under urban-like condition, using combined approaches involving chassis dynamometer
22 measurement and environmental chamber simulation. The PFI vehicle emits slightly more volatile organic
23 compounds, e.g., benzene and toluene, whereas the GDI vehicle emits more particulate components, e.g., the total
24 PM, elemental carbon, primary organic aerosols and polycyclic aromatic hydrocarbons. Strikingly, a much higher
25 SOA production (by a factor of approximately 2.7) is found from the exhaust of the GDI vehicle than that of the



26 PFI vehicle under the same conditions. More importantly, the higher SOA production found in the GDI vehicle
27 exhaust occurs concurrently with lower concentrations of traditional SOA precursors, e.g., benzene and toluene,
28 indicating a greater contribution of intermediate volatility organic compounds and semivolatile organic compounds
29 in the GDI vehicle exhaust to the SOA formation. Our results highlight the considerable potential contribution of
30 GDI vehicles to urban air pollution in the future.

31

32

33 **Introduction**

34 Organic aerosols account for approximately 20-50 % of ambient fine particulate matter (PM_{2.5}), with
35 significant environment and health effects (Kanakidou et al., 2005). Primary organic aerosol (POA) is emitted
36 directly by sources, while secondary organic aerosol (SOA) is mainly formed via oxidation of gaseous precursors
37 in the atmosphere and account for about 30-90 % of the organic aerosol (OA) mass worldwide (Zhang et al., 2007;
38 Hu et al., 2016). A recent study revealed that 15-65 % of SOA was contributed by fossil fuel consumption (i.e.,
39 traffic and coal burning) in megacities, which indicates the important contribution of vehicles to ambient SOA in
40 urban areas (Huang et al., 2014). An ambient organic aerosol measurement in the Los Angeles Basin demonstrated
41 that SOA contributed from gasoline vehicles was significant in the urban air, much larger than that from diesel
42 vehicles (Bahreini et al., 2012). Meanwhile, several chamber simulation studies concluded that exhausts of gasoline
43 vehicles could form substantial SOA (Jathar et al., 2014). Thus, gasoline vehicles exhaust is highly associated with
44 ambient SOA formation.

45 Gasoline vehicles can be categorized into two types based on the fuel injection technologies in their engine,
46 i.e., port fuel injection (PFI) vehicles and gasoline direct injection (GDI) vehicles. Unlike a PFI engine, in which
47 gasoline is injected into intake port, gasoline is sprayed into cylinder directly in a GDI engine. With the increased
48 atomization and vaporization rate of fuel, and more accurate control of fuel volume and injection time, a GDI
49 engine improves fuel efficiency and reduces CO₂ emissions (Myung et al., 2012; Liang et al., 2013). In past decades,
50 PFI vehicles dominated the market share of gasoline cars in the world. However, in recent years, GDI vehicles have



51 been increasingly employed, due to their higher fuel efficiency. The market share of GDI vehicles in 2016 reached
52 about 25 %, 50 % and 60 % in China, the US and Europe, respectively (Wen et al., 2016; Zimmerman et al., 2016).

53 Several previous studies investigated the emissions of GDI and PFI vehicles, in terms of concentrations of
54 gaseous pollutants, particle numbers and mass concentrations, and evaluated the reduction of emissions with the
55 upgrading emission standards (Ueberall et al., 2015; Zhu et al., 2016; Saliba et al., 2017). These studies show that
56 GDI vehicles emit more primary particles than PFI vehicles (Zhu et al., 2016; Saliba et al., 2017), and even diesel
57 vehicles equipped with diesel particulate filter (DPF) (Wang et al., 2016), which is likely due to insufficient time
58 allowed for gasoline fuel to be mixed with air thoroughly, as well as gasoline droplets impinging onto pistons and
59 surfaces of combustion chamber in GDI engine (Chen et al., 2017; Fu et al., 2017). However, in most studies,
60 vehicles were tested under the driving cycles of the US or European standards, indicating that those results are not
61 representative of China's traffic conditions.

62 SOA production from gasoline vehicle exhaust was previously simulated in smog chambers and potential
63 aerosol mass (PAM) flow reactors. SOA formed from gaseous pollutants exceeds the related POA emissions and
64 having much more contribution to air quality degradation. These studies mostly focused on the impacts of SOA
65 formation by the model year (Gordon et al., 2014; Jathar et al., 2014; Liu et al., 2015), fuel formulations (Peng et
66 al., 2017), driving cycles (including idling) (Nordin et al., 2013) and start-up modes of the gasoline
67 vehicles (Gentner et al., 2017). Few studies, however, have investigated SOA formation from vehicles with different
68 engine technologies (GDI and PFI) under the same working condition.

69 In this study, both primary emissions and secondary aerosol formation from GDI and PFI vehicles were
70 investigated. To represent typical urban driving patterns in megacities such as Beijing, the vehicles were tested
71 using gasoline fuel meeting the China Phase V fuel standard, and were operated with the cold-start Beijing cycle
72 (BJC). The SOA formations from both the PFI and GDI vehicle exhausts were then simulated using a smog chamber.
73 Finally, the overall contributions of the GDI and PFI gasoline vehicles to ambient particulate matter (PM) were
74 evaluated. This study is part of a project that investigates the relationship between vehicle (engine) emissions and
75 ambient aerosols, including potential of SOA formation from a PFI engine (Du et al., 2017) and the effects of



76 gasoline aromatics on SOA formation (Peng et al., 2017).

77

78 **2 Materials and methods**

79 **2.1 Vehicles**

80 One PFI vehicle and one GDI vehicle were tested in this study to investigate their primary emissions and SOA
81 formations. In this study, the selected PFI and GDI vehicles were certified to the China Phase IV Emissions
82 Standard (equivalent to Euro IV) and the China Phase V Emissions Standard (equivalent to Euro V), respectively.
83 More information of the vehicles is shown in Table 1. The fuel used in the experiments was a typical Phase V
84 gasoline on the China market. Cold-start BJC, characterized by a higher proportion of idling periods and lower
85 acceleration speeds than the New European Driving Cycle (NEDC), was performed to simulate the repeated braking
86 and acceleration on road in megacities such as Beijing. The BJC lasted approximately 17 minutes, with a maximum
87 speed of 50 km h⁻¹ (Peng et al., 2017).

88

89 **2.2 Experimental setup**

90 The chamber experiments were carried out in the summer at the State Key Laboratory of Automotive Safety
91 and Energy of Tsinghua University in Beijing. The tested vehicles were placed on a chassis dynamometer system
92 (Burke E. Porter Machinery Company) with a controlled room temperature and absolute humidity of 26.4±2.5 °C
93 and 11.5±2.4 g m⁻³, respectively. The exhaust emitted by the vehicle tailpipe was diluted in a constant volume
94 sampler (CVS) system, where the flow was maintained at 5.5 m³ min⁻¹ using filtered ambient air, achieving about
95 20 times dilution of the exhaust. Several instruments, including an AVL CEBII gas analyzer, a Cambustion
96 Differential Mobility Spectrometer (DMS500) and a particle sampler, were connected to the CVS (detailed in
97 Figure 1 and section 2.3) to characterize the primary gas- and particulate-phase pollutants. The diluted exhausts
98 produced by the CVS system were injected into an outdoor chamber, where secondary aerosol formation from
99 gasoline vehicle exhausts was simulated. This was the second dilution step of the exhausts and had a dilution factor
100 of approximately 15. A schematic illustration of the outdoor experimental setup is shown in Figure 1.



101 The photochemical oxidation experiments were carried out in a quasi-atmospheric aerosol evolution study
102 (QUALITY) outdoor chamber. More details of the setup and performance of the QUALITY chamber were
103 introduced by Peng et al. (2017). Prior to each experiment, the chamber was covered with a double-layer anti-
104 ultraviolet (anti-UV) shade to block sunlight and was cleaned with zero air for about 15 h to create a clean
105 environment. Approximately 120 ppb O₃ were injected into the chamber prior to the injection of vehicle exhaust to
106 make the oxidation environment similar to the mean O₃ peak concentration in the ambient atmosphere. Before the
107 chamber was exposed to sunlight, about 15-minute period was left to ensure that the pollutants mixed sufficiently
108 in the chamber, then the initial concentrations were characterized in the dark. Subsequently, the anti-UV shade
109 were removed from the chamber and photo-oxidation was initiated. A suite of high time resolution instruments was
110 utilized to track the evolution of pollutants during the chamber experiments. Zero air was added into the chamber
111 when sampling to maintain a constant pressure.

112

113 2.3 Instrumentation

114 Primary gases and aerosols were measured by the instruments connected to the CVS. The concentrations of
115 gaseous pollutants, including CO, CO₂, NO_x and total hydrocarbon (THC) were monitored with a gas analyzer
116 AVL Combustion Emissions Bench II (CEB II, AVL, Austria). Primary aerosols were measured with both on-line
117 and off-line instruments. A DMS500 (Cambustion, UK) was implemented to monitor the real-time number size
118 distribution and total number concentration of primary particles. The aerosols were also collected on Teflon and
119 quartz filters by AVL Particulate Sampling System (SPC472, AVL, Austria) to analyze the mass, organic carbon
120 (OC) and elemental carbon (EC) emission factors using a balance and OC/EC analyzer (Sunset Lab, USA).

121 During the chamber experiments, a suite of real-time instruments was utilized to characterize the evolutions
122 of the gas and particulate-phase pollutants. CO analyzer, NO-NO₂-NO_x analyzer and O₃ analyzer (Thermo Fisher
123 Scientific Inc., USA) were employed to measure the concentrations of CO, NO_x (including NO and NO₂) and O₃,
124 respectively. The evolutions of volatile organic compounds (VOCs) were monitored with a proton transfer reaction
125 mass spectrometer (PTR-MS, IoniconAnalytik, Austria) (Lindinger et al., 1998). H₃O⁺ was used as the reagent ion,



126 which reacted with the target compounds. The resulting ions were detected by a quadruple mass spectrometer.
127 Meanwhile, the particles size distribution was characterized using a scanning mobility particle sizer system (SMPS,
128 TSI, USA), which consisted of a differential mobility analyzer (DMA, TSI, USA) and a condensation particle
129 counter (CPC, TSI, USA). This system can measure aerosols with a diameters ranging from 15 nm to 700 nm. A
130 high-resolution time-of-flight aerosol mass spectrometer (HR-Tof-AMS, Aerodyne Research, USA) was applied to
131 obtain mass concentrations and size distributions of submicron, non-refractory aerosols, including sulfate, nitrate,
132 ammonium, chloride and organic (DeCarlo et al., 2006). Table 2 lists the instruments used to measure the primary
133 emissions and their evolutions in the chamber experiments.

134

135 **3 Results and discussion**

136 **3.1 Primary emissions**

137 **Gaseous pollutant emissions**

138 Emission factors (EFs) of CO₂, THC, benzene and toluene from the GDI and PFI vehicles are listed in Table
139 3. The EFs of CO₂ and THC are derived from measured concentrations in CVS, while the EFs of benzene and
140 toluene were calculated from the initial concentrations in the chamber. The THC emission factor was reported in
141 units of carbon mass, g C kg⁻¹fuel⁻¹.

142 The GDI vehicle emitted less CO₂ and THC than the PFI vehicle due to their different fuel injection strategies
143 and mixing features (Liang et al. 2013; Gao et al., 2015). The EF of THC from the GDI vehicle met the standard
144 of the China Phase V Emission Standard (0.1 g km⁻¹), but that from the PFI vehicle was slightly beyond the standard
145 limit. The PFI vehicle used in this study met lower emission standard (the China Phase IV), which might cause
146 additional THC emission when compared to the China Phase V Emission Standard. In addition, BJC and NEDC
147 were applied in this study and emission standard, respectively. More repeated braking and acceleration in BJC
148 might cause incomplete combustion and consequently higher THC emission from the PFI vehicle in this study. As
149 typical VOC species emitted by vehicles, benzene and toluene were measured in this study. For both vehicles, the
150 EFs of toluene were higher than those of benzene. Consistent with the feature of THC emission, the PFI vehicle



151 emitted more benzene and toluene than the GDI vehicle, and the enhancement of toluene was much larger than that
152 of benzene.

153 The EFs of the gaseous pollutants in this study had similar magnitudes to those in previous studies in which
154 gasoline vehicles met comparable levels of emission standards and were tested under cold-start driving condition,
155 while the results in this study were slightly higher, as shown in Table 3. This difference might be because the
156 California ultralow-emission vehicles (ULEV) (Saliba et al., 2017) and most LEV II vehicles (manufactured in
157 2004 or later) (May et al., 2014) meet the US certification gasoline emission standards for the ULEV category,
158 which has a lower limit of gaseous pollutants than the China Phase V Emission Standard. In addition, the different
159 driving cycles of our study and those other studies (listed in Table 3) might be another explanation for the difference
160 in the EFs of gaseous pollutants.

161 **Primary particle emissions**

162 The EFs of PM, elemental carbon (EC), POA and particulate polycyclic aromatic hydrocarbons (PAHs) are
163 shown in Table 4. The EF of PM_{2.5} from the GDI vehicle was about 1.4 times higher than that of the PFI vehicle.
164 Both vehicles met the China Phase V Emission Standard for PM emission (4.5 mg km⁻¹). The GDI vehicle emitted
165 about 3.3 times more EC and 1.2 times more POA than the PFI vehicle. The primary carbonaceous aerosols
166 (EC+POA) accounted for 85 % and 82 % of the PM in the GDI and PFI vehicles respectively, suggesting that
167 carbonaceous aerosols were the major contributors in the PM from gasoline vehicles, especially for the GDI vehicle.

168 PAHs account for a small fraction of particulate organic matter in the atmosphere, but the molecular signature
169 of PAHs can be utilized in source identification of vehicle emissions (Kamal et al., 2015). The GDI vehicle emitted
170 about 1.5 times the PAHs of the PFI vehicle. It should be noted that the PAHs were tested under warm-start cycles.
171 A higher EF of PAHs would be obtained under cold-start cycle, since the lower temperature led to inefficient
172 catalyst at the beginning of cold-start (Mathis et al., 2005).

173 The higher PM_{2.5} and carbonaceous aerosol emissions from GDI vehicle were also found in Saliba's and
174 Zhu's studies (Zhu et al., 2016; Saliba et al., 2017). The EC emissions were in the range of those of previous studies
175 but on the lower level. The EF of the POA measured in this study was higher than those of other studies, leading



176 to a higher OC/EC ratio, which could be attributed to the less strict emission standard of our vehicles and the
177 different driving cycles applied in the experiments.

178 The bimodal number size distributions of the primary PM from the vehicles measured by the DMS500 are
179 shown in Figure 2. The particle distributions of the exhausts of the GDI and PFI vehicles illustrated similar patterns,
180 with two peaks located at about 10 nm for nucleation mode and at 60-90 nm for accumulation mode, respectively,
181 which are consistent with the results of previous studies (Maricq et al., 1999; Chen et al., 2017). The bimodal
182 particle distributions from gasoline vehicles verified the traffic emission related sources resolved from ambient
183 aerosols in Beijing (Wang et al., 2013), indicating that vehicle emissions significantly contribute to the small
184 particles in the ambient air, especially those under 100 nm. The particle number size distribution of the exhausts of
185 the GDI vehicle showed a similar pattern to that of the PFI vehicle, with a much higher number concentration that
186 is consistent with the emission of more particle mass.

187

188 **3.2 SOA formation from gasoline vehicle exhaust**

189 The time-resolved concentrations of gases and particles during the chamber experiments are illustrated in
190 Figure 3. Before removing the anti-UV shade, the initial concentrations of NO_x, benzene and toluene from the PFI
191 and GDI vehicles were 80 ppb, 3 ppb, 5 ppb and 100 ppb, 4 ppb, 14 ppb respectively.

192 After the aging experiment started (t=0 in Figure 3), NO was formed from NO₂ photolysis, and then reacted
193 with O₃ to form NO₂. The O₃ concentration increased rapidly to a maximum within 2-3 h and then decreased via
194 reactions and dilution. Benzene and toluene decayed during the aging process at different rates.

195 New particle formation was found inside the chamber 15 minutes after the exhaust was exposed to sunlight,
196 providing substantial seeds for secondary aerosol formation. Significant growths of particles in both size and mass
197 were observed in the chamber, indicating that a large amount of secondary aerosol was formed during the
198 photochemical oxidation. The chemical compositions of the secondary aerosols were measured continuously by
199 HR-ToF-AMS. Organic was the dominant composition of the secondary aerosol, accounting for 88-95 % of the
200 total particle mass inside the chamber (Figure S1), which is consistent with our previous research (Peng et al.,



201 2017). The SOA mass exhibited different growth rate for the two types of vehicles. After a 4 h oxidation in the
202 chamber, the SOA formed from the exhaust of the GDI vehicle was approximately double that of the PFI vehicle.

203 The solar radiation conditions significantly influenced the SOA formation. Thus, OH exposure was used to
204 characterize the photochemical age as a normalization, instead of the experiment time. Two VOC species with
205 noticeable differences in their reaction rate constants with OH radicals could be utilized to calculate the OH
206 exposure ($[\text{OH}] \Delta t$) based on Equation 1 (for benzene and toluene, as used in this study) (Yuan et al., 2012).

$$207 \quad [\text{OH}] \Delta t = \frac{1}{k_T - k_B} \times \left(\ln \frac{[T]}{[B]} \Big|_{t=0} - \ln \frac{[T]}{[B]} \right) \quad (1)$$

208 where k_T and k_B are the OH rate constants of benzene ($1.2 \times 10^{-12} \text{ cm}^3 \text{ molecule}^{-1} \text{ s}^{-1}$) (Yuan et al., 2012) and toluene
209 ($5.5 \times 10^{-12} \text{ cm}^3 \text{ molecule}^{-1} \text{ s}^{-1}$) (Kramp and Paulson, 1998), respectively. $\frac{[T]}{[B]} \Big|_{t=0}$ is the concentration ratio of
210 toluene to benzene at the beginning of the aging process, and $\frac{[T]}{[B]}$ is their concentration ratio measured during
211 aging process.

212 The SOA concentrations as a function of OH exposure are illustrated in Figure 4. Wall-loss correction and
213 dilution correction, including both particles and gaseous pollutants, were taken into consideration in the calculation
214 of the SOA mass concentration in the chamber (Peng et al., 2017). Assuming the mean OH concentration was
215 $1.6 \times 10^6 \text{ molecular cm}^{-3}$ in Beijing (Lu et al., 2013), the whole aging procedure in the chamber experiments was
216 equal to a 6-10 h atmospheric photochemical oxidation. The average SOA concentrations were 9.25 ± 1.80 and
217 $4.68 \pm 1.32 \text{ } \mu\text{g m}^{-3}$ for the GDI and PFI vehicles, respectively, when the OH exposure was $5 \times 10^6 \text{ molecular cm}^{-3} \text{ h}$
218 in the chamber. Considering the driving cycle mileage and fuel consumption, the SOA productions were
219 $54.77 \pm 10.70 \text{ mg kg}^{-1} \text{ fuel}^{-1}$ or $3.06 \pm 0.60 \text{ mg km}^{-1}$ for the GDI vehicle and $20.57 \pm 5.82 \text{ mg kg}^{-1} \text{ fuel}^{-1}$ or $1.55 \pm 0.44 \text{ mg}$
220 km^{-1} for the PFI vehicle. Compared with the PFI vehicle, the GDI vehicle exhaust exhibited a higher potential of
221 SOA formation, even though the PFI vehicle emitted more VOCs, which are considered as dominant class of SOA
222 precursors. This result indicates that higher concentrations of some other SOA precursors exist in the exhaust of
223 GDI vehicles, which will be further discussed in section 3.3.

224 The results from chamber simulation of SOA formation from individual gasoline vehicles are illustrated in



225 Figure 5. The SOA production from the both vehicles in this study is in the range of the results of previous studies
226 (Nordin et al., 2013; Platt et al., 2013; Jathar et al., 2014; Liu et al., 2015; Peng et al., 2017). The variation of the
227 SOA production among these studies might be caused by several factors: the model years of vehicles
228 (corresponding to emission standards), their driving cycles, the initial concentrations of gaseous pollutants in the
229 chamber, and the NO_x condition of the SOA formation in the chamber experiments.

230 To investigate the dominant contributors to ambient PM from the GDI and PFI vehicles, Figure 6 illustrates
231 the EFs of EC and POA as well as the production factors of SOA in this study. The SOA production from the GDI
232 vehicle was approximately 2.7 times higher than that from the PFI vehicle. At 5 × 10⁶ molecular cm⁻³ h OH exposure,
233 the SOA/POA ratio was approximately 1. Figure 4 illustrates that the SOA production increased with
234 photochemical age rapidly (within 2 × 10⁷ molecular cm⁻³ h). Thus, SOA would exceed POA at higher OH exposure,
235 e.g., the SOA/POA ratio reached about 4 at 10⁷ molecular cm⁻³ h OH exposure, becoming the major PM contributor.
236 In terms of the POA and EC emissions as well as the SOA formation, the GDI vehicle contributed 2.2 times more
237 than the PFI vehicle.

238 Although wall-loss correction as well as particle and gas dilution corrections were considered in this study,
239 the SOA productions were still underestimated. First, the concentration of aerosols in the ambient air in Beijing
240 was higher than that inside the chamber. Semi-volatile vapors may prefer to be partitioned into particle phase rather
241 than gas phase in ambient condition, increasing the SOA formation (Odum et al., 1996). Second, the loss of semi-
242 volatile vapors to the chamber walls was not considered in the calculation of the SOA production. Previous study
243 found that semi-volatile vapor loss could lead to the underestimation of SOA formation with a factor of 1.1-4.1
244 (Zhang et al., 2014). Therefore, the SOA production from vehicle exhaust would be enhanced under atmospheric
245 condition.

246

247 3.3 SOA mass closure

248 SOA production ($\Delta OA_{\text{predicted}}$) estimated from VOC precursors can be defined as Eq. (2):

$$249 \Delta OA_{\text{predicted}} = \sum_i (\Delta_i \times Y_i) \quad (2)$$



250 where Δ_i is the concentration change of precursor VOC_i measured with PTR-MS in the chamber experiments, and
251 Y_i is the SOA yield of the VOC_i . In this study, benzene, toluene, C8 benzene and C9 benzene were involved in the
252 estimation of SOA production, and alkanes and alkenes were not considered because much lower declines of
253 concentrations were observed than those of aromatics during chamber experiments.

254 The SOA yield is sensitive to VOCs/NO_x ratio (Song et al., 2005). In this study, the VOCs/NO_x ratio was in
255 the range of 0.5-1.0, thus, the SOA formation from the vehicle exhaust was determined under high NO_x conditions.
256 The high NO_x SOA yields of benzene and toluene were taken from Ng et al. (2007). The C8 and C9 benzene used
257 the SOA yield of m-xylene from Platt et al. (2013).

258 The increased predicted SOA contribution from the VOC precursors as a function of OH exposure
259 accumulation is demonstrated in Figure 7. At the end of the experiments, the SOA estimated from these speciated
260 VOCs accounted for about 25 % and 53 % of the measured SOA formation from the GDI and PFI vehicle exhausts,
261 respectively. Similar to the results of previous studies (Platt et al., 2013; Nordin et al., 2013; Gordon et al., 2014),
262 single-ring aromatics played an important role in the SOA formation, especially for the PFI vehicle which shows
263 higher predicted SOA fraction.

264 The unpredicted fraction of the measured SOA in the chamber experiments was in the range of 47-75 %.
265 Contributions from intermediate volatility organic compounds (IVOCs) and semivolatile organic compounds
266 (SVOCs), e.g., long branched and cyclic alkanes and gas-phase polycyclic aromatic hydrocarbons could be a
267 possible explanation for this underestimation. The SOA formed by oxidation of IVOCs and SVOCs is found to
268 dominate over that from single-ring aromatics (Robinson et al., 2007). The unpredicted SOA ratio exhibited a
269 maximum value at the beginning of the experiment, indicating that the IVOCs and SVOCs with low volatilities
270 produced SOA much more efficiently than the single-ring aromatics with high volatilities, as the first generation
271 products of photo-oxidation of these precursors form SOA (Robinson et al., 2007).

272 The larger fraction of the unpredicted SOA from the GDI vehicle exhaust might be associated with higher
273 IVOCs and SVOCs emissions. Gas-phase PAH is one of the main component of speciated IVOCs (Zhao et al.,
274 2016). The particulate-phase PAHs from the GDI vehicle were more abundant than those from the PFI vehicle by



275 a factor of 1.5 (section 3.1). Based on gas-particle equilibrium, this indicates that more gas-phase PAHs, including
276 some aromatic IVOCs, might be emitted by the GDI vehicles, contributing to the SOA enhancement.

277

278 **4 Discussions and conclusions**

279 GDI and PFI vehicles have different fuel injection technologies in their engines, which affects their emissions
280 of gaseous and particulate pollutants. In GDI engine, the fuel is directly injected into cylinder, which benefits the
281 fuel atomization and vaporization and provides better control of fuel volume and the combustion process (Liang et
282 al. 2013; Gao et al., 2015). Thus, in this study, the tested GDI vehicle has higher fuel economy and lower THC
283 emission than the PFI vehicle. However, the insufficient mixing time allowed for the fuel and air leads to
284 incomplete combustion in the GDI engine (Fu et al., 2014). In addition, direct fuel injection leads to fuel
285 impingement onto surfaces of combustion chamber, where liquid pools form, favoring soot-like particulate
286 formation (Ueberall et al., 2015; Chen et al., 2017). Consequently, larger particle mass and number are emitted by
287 the GDI vehicle than from the PFI vehicle. The particles emitted by the GDI vehicle have higher EC mass fraction,
288 leading to lower OC/EC ratio. The considerable particle number emitted by gasoline vehicles, especially in GDI
289 vehicles exhaust, makes a significant contribution to particle number concentration as well as seeds for further
290 reactions in the atmosphere, and needs to be controlled in the future emission standards.

291 Our results show that the GDI vehicle contributes more to both primary and secondary aerosol than the PFI
292 vehicle, and has greater impact on environment and air quality. In recent years, the market share of GDI vehicles
293 exerts a continuous growth in China because they provide better fuel economy and lower CO₂ emissions. In 2016,
294 GDI vehicles accounted for 25 % of China's market share, and this proportion is expected to reach 60 % by 2020
295 (Wen et al., 2016). The PM enhancement of GDI vehicles with increasing population could potentially offset any
296 PM emission reduction benefits, including the development of gasoline emission and fuel standards and the
297 advanced engine technologies of gasoline vehicles. Therefore, our results highlight the necessity of further research
298 and regulation of GDI vehicles.

299 Primary emissions and secondary organic formation from one GDI vehicle and one PFI vehicle were



300 investigated when driving under cold-start BJC. The primary PM emitted by the GDI vehicle was 1.4 times greater
301 than that from the PFI vehicle and the SOA formation from the GDI vehicle exhaust was 2.7 times greater than that
302 from the PFI vehicle exhaust for the same OH exposure. The SOA production factors were 54.77 ± 10.70 mg kg⁻¹
303 fuel⁻¹ or 3.06 ± 0.60 mg km⁻¹ for the GDI vehicle and 20.57 ± 5.82 mg kg-fuel⁻¹ or 1.55 ± 0.44 mg km⁻¹ for the PFI
304 vehicle at an OH exposure of 5×10^6 molecular cm⁻³ h, which is consistent with the values seen in previous studies.
305 Considering the higher amounts of OA derived from primary emission and secondary formation, the GDI vehicle
306 contribute considerably more to particle mass concentrations in the ambient air than the PFI vehicle.

307 The SOA formation was predicted from the gaseous precursors emitted by the GDI and PFI vehicles under
308 high NO_x condition. Single-ring aromatic VOCs could explain only 25-53 % of the measured SOA formation in
309 the chamber experiments. The GDI vehicle exhibited higher fraction of unexplained SOA. More IVOCs and
310 SVOCs were inferred as being emitted by the GDI vehicle.

311 With increasing population of GDI vehicles, any benefits of the aerosol emission reduction of gasoline
312 vehicles are substantially offset, because GDI vehicles have significant contributions to ambient aerosols. More
313 work is needed to improve the understanding of GDI vehicle emissions and to provide information for the
314 regulation of gasoline vehicles.

315

316

317 *Data availability.* The data presented in this article are available from the authors upon request
318 (minhu@pku.edu.cn).

319

320

321 **Acknowledgments**

322 This work was supported by the National Basic Research Program of China (973 Program) (2013CB228503,
323 2013CB228502), National Natural Science Foundation of China (91544214, 41421064, 51636003), the Strategic
324 Priority Research Program of Chinese Academy of Sciences (XDB05010500), and China Postdoctoral Science



325 Foundation (2015M580929). We also thank the State Key Lab of Automotive Safety and Energy at Tsinghua
326 University for the support to experiments.
327

328 **Reference**

- 329 Bahreini, R., Middlebrook, A. M., de Gouw, J. A., Warneke, C., Trainer, M., Brock, C. A., Stark, H., Brown, S. S.,
330 Dube, W. P., Gilman, J. B., Hall, K., Holloway, J. S., Kuster, W. C., Perring, A. E., Prevot, A. S. H., Schwarz, J. P.,
331 Spackman, J. R., Szidat, S., Wagner, N. L., Weber, R. J., Zotter, P., and Parrish, D. D.: Gasoline emissions dominate
332 over diesel in formation of secondary organic aerosol mass, *Geophysical Research Letters*, 39,
333 10.1029/2011gl050718, 2012.
- 334 Chen, L., Liang, Z., Zhang, X., and Shuai, S.: Characterizing particulate matter emissions from GDI and PFI
335 vehicles under transient and cold start conditions, *Fuel*, 189, 131-140, 10.1016/j.fuel.2016.10.055, 2017.
- 336 DeCarlo, P. F., Kimmel, J. R., Trimborn, A., Northway, M. J., Jayne, J. T., Aiken, A. C., Gonin, M., Fuhrer, K.,
337 Horvath, T., Docherty, K. S., Worsnop, D. R., and Jimenez, J. L.: Field-deployable, high-resolution, time-of-flight
338 aerosol mass spectrometer, *Analytical Chemistry*, 78, 8281-8289, 10.1021/ac061249n, 2006.
- 339 Du, Z., Hu, M., Peng, J., Guo, S., Zheng, R., Zheng, J., Shang, D., Qin, Y., Niu, H., Li, M., Yang, Y., Lu, S., Wu,
340 Y., Shao, M., and Shuai, S.: Potential of secondary aerosol formation from Chinese gasoline engine exhaust, *Journal*
341 *of environmental sciences*, 2017, in press.
- 342 Fu, H., Wang, Y., Li, X., and Shuai, S.: Impacts of Cold-Start and Gasoline RON on Particulate Emission from
343 Vehicles Powered by GDI and PFI Engines, *SAE Technical Paper*, 2014-01-2836, 10.4271/2014-01-2836, 2014.
- 344 Gao, Z., Curran, S. J., Parks, J. E., II, Smith, D. E., Wagner, R. M., Daw, C. S., Edwards, K. D., and Thomas, J. F.:
345 Drive cycle simulation of high efficiency combustions on fuel economy and exhaust properties in light-duty
346 vehicles, *Applied Energy*, 157, 762-776, 10.1016/j.apenergy.2015.03.070, 2015.
- 347 Gentner, D. R., Jathar, S. H., Gordon, T. D., Bahreini, R., Day, D. A., El Haddad, I., Hayes, P. L., Pieber, S. M.,
348 Platt, S. M., de Gouw, J., Goldstein, A. H., Harley, R. A., Jimenez, J. L., Prevot, A. S. H., and Robinson, A. L.:
349 Review of Urban Secondary Organic Aerosol Formation from Gasoline and Diesel Motor Vehicle Emissions,
350 *Environmental science & technology*, 51, 1074-1093, 10.1021/acs.est.6b04509, 2017.
- 351 Gordon, T. D., Presto, A. A., May, A. A., Nguyen, N. T., Lipsky, E. M., Donahue, N. M., Gutierrez, A., Zhang, M.,
352 Maddox, C., Rieger, P., Chattopadhyay, S., Maldonado, H., Maricq, M. M., and Robinson, A. L.: Secondary organic



353 aerosol formation exceeds primary particulate matter emissions for light-duty gasoline vehicles, *Atmos. Chem.*
354 *Phys.*, 14, 4661-4678, 10.5194/acp-14-4661-2014, 2014.

355 Hu, W., Hu, M., Hu, W., Jimenez, J. L., Yuan, B., Chen, W., Wang, M., Wu, Y., Chen, C., Wang, Z., Peng, J., Zeng,
356 L., and Shao, M.: Chemical composition, sources, and aging process of submicron aerosols in Beijing: Contrast
357 between summer and winter, *Journal of Geophysical Research-Atmospheres*, 121, 1955-1977,
358 10.1002/2015jd024020, 2016.

359 Huang, R.-J., Zhang, Y., Bozzetti, C., Ho, K.-F., Cao, J.-J., Han, Y., Daellenbach, K. R., Slowik, J. G., Platt, S. M.,
360 Canonaco, F., Zotter, P., Wolf, R., Pieber, S. M., Bruns, E. A., Crippa, M., Ciarelli, G., Piazzalunga, A.,
361 Schwikowski, M., Abbaszade, G., Schnelle-Kreis, J., Zimmermann, R., An, Z., Szidat, S., Baltensperger, U.,
362 Haddad, I. E., and Prévôt, A. S. H.: High secondary aerosol contribution to particulate pollution during haze events
363 in China, *Nature*, 10.1038/nature13774, 2014.

364 Jathar, S. H., Gordon, T. D., Hennigan, C. J., Pye, H. O. T., Pouliot, G., Adams, P. J., Donahue, N. M., and Robinson,
365 A. L.: Unspeciated organic emissions from combustion sources and their influence on the secondary organic aerosol
366 budget in the United States, *Proc. Natl. Acad. Sci. USA*, 111, 10473-10478, 10.1073/pnas.1323740111, 2014.

367 Kamal, A., Cincinelli, A., Martellini, T., and Malik, R. N.: A review of PAH exposure from the combustion of
368 biomass fuel and their less surveyed effect on the blood parameters, *Environmental Science and Pollution Research*,
369 22, 4076-4098, 10.1007/s11356-014-3748-0, 2015.

370 Kanakidou, M., Seinfeld, J. H., Pandis, S. N., Barnes, I., Dentener, F. J., Facchini, M. C., Van Dingenen, R., Ervens,
371 B., Nenes, A., Nielsen, C. J., Swietlicki, E., Putaud, J. P., Balkanski, Y., Fuzzi, S., Horth, J., Moortgat, G. K.,
372 Winterhalter, R., Myhre, C. E. L., Tsigaridis, K., Vignati, E., Stephanou, E. G., and Wilson, J.: Organic aerosol and
373 global climate modelling: a review, *Atmospheric Chemistry and Physics*, 5, 1053-1123, 2005.

374 Kramp, F., and Paulson, S. E.: On the uncertainties in the rate coefficients for OH reactions with hydrocarbons, and
375 the rate coefficients of the 1,3,5-trimethylbenzene and m-xylene reactions with OH radicals in the gas phase,
376 *Journal of Physical Chemistry A*, 102, 2685-2690, 10.1021/jp973289o, 1998.



- 377 Liang, B., Ge, Y., Tan, J., Han, X., Gao, L., Hao, L., Ye, W., and Dai, P.: Comparison of PM emissions from a
378 gasoline direct injected (GDI) vehicle and a port fuel injected (PFI) vehicle measured by electrical low pressure
379 impactor (ELPI) with two fuels: Gasoline and M15 methanol gasoline, *Journal of Aerosol Science*, 57, 22-31,
380 10.1016/j.jaerosci.2012.11.008, 2013.
- 381 Lindinger, W., Hansel, A., and Jordan, A.: On-line monitoring of volatile organic compounds at pptv levels by
382 means of proton-transfer-reaction mass spectrometry (PTR-MS) - Medical applications, food control and
383 environmental research, *International Journal of Mass Spectrometry*, 173, 191-241, 10.1016/s0168-
384 1176(97)00281-4, 1998.
- 385 Liu, T., Wang, X., Deng, W., Hu, Q., Ding, X., Zhang, Y., He, Q., Zhang, Z., Lü S., Bi, X., Chen, J., and Yu, J.:
386 Secondary organic aerosol formation from photochemical aging of light-duty gasoline vehicle exhausts in a smog
387 chamber, *Atmos. Chem. Phys.*, 15, 9049-9062, 10.5194/acp-15-9049-2015, 2015.
- 388 Lu, K. D., Hofzumahaus, A., Holland, F., Bohn, B., Brauers, T., Fuchs, H., Hu, M., Häsel, R., Kita, K., Kondo,
389 Y., Li, X., Lou, S. R., Oebel, A., Shao, M., Zeng, L. M., Wahner, A., Zhu, T., Zhang, Y. H., and Rohrer, F.: Missing
390 OH source in a suburban environment near Beijing: observed and modelled OH and HO₂
391 concentrations in summer 2006, *Atmos. Chem. Phys.*, 13, 1057-1080, 10.5194/acp-13-1057-2013, 2013.
- 392 Maricq, M. M., Podsiadlik, D. H., and Chase, R. E.: Gasoline vehicle particle size distributions: Comparison of
393 steady state, FTP, and US06 measurements, *Environmental science & technology*, 33, 2007-2015,
394 10.1021/es981005n, 1999.
- 395 Mathis, U., Mohr, M., and Forss, A. M.: Comprehensive particle characterization of modern gasoline and diesel
396 passenger cars at low ambient temperatures, *Atmospheric Environment*, 39, 107-117,
397 10.1016/j.atmosenv.2004.09.029, 2005.
- 398 May, A. A., Nguyen, N. T., Presto, A. A., Gordon, T. D., Lipsky, E. M., Karve, M., Gutierrez, A., Robertson, W. H.,
399 Zhang, M., Brandow, C., Chang, O., Chen, S., Cicero-Fernandez, P., Dinkins, L., Fuentes, M., Huang, S.-M., Ling,
400 R., Long, J., Maddox, C., Massetti, J., McCauley, E., Miguel, A., Na, K., Ong, R., Pang, Y., Rieger, P., Sax, T., Tin,
401 T., Thu, V., Chattopadhyay, S., Maldonado, H., Maricq, M. M., and Robinson, A. L.: Gas- and particle-phase



- 402 primary emissions from in-use, on-road gasoline and diesel vehicles, *Atmospheric Environment*, 88, 247-260,
403 10.1016/j.atmosenv.2014.01.046, 2014.
- 404 Myung, C.-L., Kim, J., Choi, K., Hwang, I. G., and Park, S.: Comparative study of engine control strategies for
405 particulate emissions from direct injection light-duty vehicle fueled with gasoline and liquid phase liquefied
406 petroleum gas (LPG), *Fuel*, 94, 348-355, 10.1016/j.fuel.2011.10.041, 2012.
- 407 Ng, N. L., Kroll, J. H., Chan, A. W. H., Chhabra, P. S., Flagan, R. C., and Seinfeld, J. H.: Secondary organic aerosol
408 formation from m-xylene, toluene, and benzene, *Atmos. Chem. Phys.*, 7, 3909–3922, 2007.
- 409 Nordin, E. Z., Eriksson, A. C., Roldin, P., Nilsson, P. T., Carlsson, J. E., Kajos, M. K., Hellén, H., Wittbom, C.,
410 Rissler, J., Löndahl, J., Swietlicki, E., Svenningsson, B., Bohgard, M., Kulmala, M., Hallquist, M., and Pagels, J.
411 H.: Secondary organic aerosol formation from idling gasoline passenger vehicle emissions investigated in a smog
412 chamber, *Atmos. Chem. Phys.*, 13, 6101-6116, 10.5194/acp-13-6101-2013, 2013.
- 413 Odum, J. R., Hoffmann, T., Bowman, F., Collins, D., Flagan, R. C., and Seinfeld, J. H.: Gas/particle partitioning
414 and secondary organic aerosol yields, *Environ. Sci. Technol.*, 30, 2580-2585, 10.1021/es950943+, 1996.
- 415 Peng, J., Hu, M., Du, Z., Wang, Y., Zheng, J., Zhang, W., Yang, Y., Qin, Y., Zheng, R., Xiao, Y., Wu, Y., Lu, S., Wu,
416 Z., Guo, S., Mao, H., and Shuai, S.: Gasoline aromatic: a critical determinant of urban secondary organic aerosol
417 formation, *Atmospheric Chemistry and Physics*, 2017, in press.
- 418 Platt, S. M., El Haddad, I., Zardini, A. A., Clairotte, M., Astorga, C., Wolf, R., Slowik, J. G., Temime-Roussel, B.,
419 Marchand, N., Ježek, I., Drinovec, L., Močnik, G., Möhler, O., Richter, R., Barmet, P., Bianchi, F., Baltensperger,
420 U., and Prévôt, A. S. H.: Secondary organic aerosol formation from gasoline vehicle emissions in a new mobile
421 environmental reaction chamber, *Atmos. Chem. Phys.*, 13, 9141-9158, 10.5194/acp-13-9141-2013, 2013.
- 422 Robinson, A. L., Donahue, N. M., Shrivastava, M. K., Weitkamp, E. A., Sage, A. M., Grieshop, A. P., Lane, T. E.,
423 Pierce, J. R., and Pandis, S. N.: Rethinking organic aerosols: Semivolatile emissions and photochemical aging,
424 *Science*, 315, 1259-1262, 10.1126/science.1133061, 2007.
- 425 Saliba, G., Saleh, R., Zhao, Y., Presto, A. A., Lambe, A. T., Frodin, B., Sardar, S., Maldonado, H., Maddox, C.,
426 May, A. A., Drozd, G. T., Goldstein, A. H., Russell, L. M., Hagen, F., and Robinson, A. L.: Comparison of Gasoline



- 427 Direct-Injection (GDI) and Port Fuel Injection (PFI) Vehicle Emissions: Emission Certification Standards, Cold-
428 Start, Secondary Organic Aerosol Formation Potential, and Potential Climate Impacts, *Environmental science &*
429 *technology*, 51, 6542-6552, 10.1021/acs.est.6b06509, 2017.
- 430 Song, C., Na, K. S., and Cocker, D. R.: Impact of the hydrocarbon to NO_x ratio on secondary organic aerosol
431 formation, *Environ. Sci. Technol.*, 39, 3143-3149, 10.1021/es0493244, 2005.
- 432 Ueberall, A., Otte, R., Eilts, P., and Krahl, J.: A literature research about particle emissions from engines with direct
433 gasoline injection and the potential to reduce these emissions, *Fuel*, 147, 203-207, 10.1016/j.fuel.2015.01.012,
434 2015.
- 435 Wang, Y., Zheng, R., Qin, Y., Peng, J., Li, M., Lei, J., Wu, Y., Hu, M., and Shuai, S.: The impact of fuel compositions
436 on the particulate emissions of direct injection gasoline engine, *Fuel*, 166, 543-552, 10.1016/j.fuel.2015.11.019,
437 2016.
- 438 Wang, Z. B., Hu, M., Wu, Z. J., Yue, D. L., He, L. Y., Huang, X. F., Liu, X. G., and Wiedensohler, A.: Long-term
439 measurements of particle number size distributions and the relationships with air mass history and source
440 apportionment in the summer of Beijing, *Atmospheric Chemistry and Physics*, 13, 10159-10170, 10.5194/acp-13-
441 10159-2013, 2013.
- 442 Wen, Y., Wang, Y., Fu, C., Deng, W., Zhan, Z., Tang, Y., Li, X., Ding, H., and Shuai, S.: The Impact of Injector
443 Deposits on Spray and Particulate Emission of Advanced Gasoline Direct Injection Vehicle, *SAE Technical Paper*,
444 2016-01-2284, 10.4271/2016-01-2284, 2016.
- 445 Yuan, B., Shao, M., de Gouw, J., Parrish, D. D., Lu, S., Wang, M., Zeng, L., Zhang, Q., Song, Y., Zhang, J., and
446 Hu, M.: Volatile organic compounds (VOCs) in urban air: How chemistry affects the interpretation of positive
447 matrix factorization (PMF) analysis, *Journal of Geophysical Research: Atmospheres*, 117, n/a-n/a,
448 10.1029/2012jd018236, 2012.
- 449 Zhang, Q., Jimenez, J. L., Canagaratna, M. R., Allan, J. D., Coe, H., Ulbrich, I., Alfarra, M. R., Takami, A.,
450 Middlebrook, A. M., Sun, Y. L., Dzepina, K., Dunlea, E., Docherty, K., DeCarlo, P. F., Salcedo, D., Onasch, T.,
451 Jayne, J. T., Miyoshi, T., Shimon, A., Hatakeyama, S., Takegawa, N., Kondo, Y., Schneider, J., Drewnick, F.,



- 452 Borrmann, S., Weimer, S., Demerjian, K., Williams, P., Bower, K., Bahreini, R., Cottrell, L., Griffin, R. J.,
453 Rautiainen, J., Sun, J. Y., Zhang, Y. M., and Worsnop, D. R.: Ubiquity and dominance of oxygenated species in
454 organic aerosols in anthropogenically-influenced Northern Hemisphere midlatitudes, *Geophysical Research Letters*,
455 34, 10.1029/2007gl029979, 2007.
- 456 Zhang, X., Cappa, C. D., Jathar, S. H., McVay, R. C., Ensberg, J. J., Kleeman, M. J., and Seinfeld, J. H.: Influence
457 of vapor wall loss in laboratory chambers on yields of secondary organic aerosol, *Proc. Natl. Acad. Sci. USA*, 111,
458 5802-5807, 10.1073/pnas.1404727111, 2014.
- 459 Zhao, Y., Nguyen, N. T., Presto, A. A., Hennigan, C. J., May, A. A., and Robinson, A. L.: Intermediate Volatility
460 Organic Compound Emissions from On-Road Gasoline Vehicles and Small Off-Road Gasoline Engines,
461 *Environmental science & technology*, 50, 4554-4563, 10.1021/acs.est.5b06247, 2016.
- 462 Zhu, R., Hu, J., Bao, X., He, L., Lai, Y., Zu, L., Li, Y., and Su, S.: Tailpipe emissions from gasoline direct injection
463 (GDI) and port fuel injection (PFI) vehicles at both low and high ambient temperatures, *Environmental Pollution*,
464 216, 223-234, 10.1016/j.envpol.2016.05.066, 2016.
- 465 Zimmerman, N., Wang, J. M., Jeong, C.-H., Ramos, M., Hilker, N., Healy, R. M., Sabaliauskas, K., Wallace, J. S.,
466 and Evans, G. J.: Field Measurements of Gasoline Direct Injection Emission Factors: Spatial and Seasonal
467 Variability, *Environmental science & technology*, 50, 2035-2043, 10.1021/acs.est.5b04444, 2016.
- 468



469 Table 1 Descriptions of the gasoline direct injection (GDI) and port fuel injection (PFI) vehicles used in the
470 experiments.

Vehicle	Make and model	Emission standard class	Model year	Mileage (km)	Displacement (cm ³)	Power (kW)	Weight (kg)
GDI	VW Sagitar	China V	2015	3000	1395	110	1395
PFI	Honda Civic	China IV	2009	42500	1799	103	1280

471



472 Table 2 Overview of all instruments used to measure the gas and particulate phase pollutants in the experiments.

Parameter	Phase	Instrument	Note
CO, CO ₂ , NO _x and total hydrocarbon concentration	Gas	Gas analyzer AVL Combustion Emissions Bench II	On-line
Aerosol number size distribution	Particle	DMS500	On-line
PM _{2.5}	Particle	Balance (AX105DR)	Off-line
Organic carbon/Elemental carbon concentration	Particle	OC/EC analyzer	Off-line
CO concentration	Gas	48i CO analyzer	On-line
NO, NO ₂ , and NO _x concentration	Gas	42i NO-NO ₂ -NO _x analyzer	On-line
O ₃ concentration	Gas	49i O ₃ analyzer	On-line
VOCs concentration	Gas	Proton transfer reaction mass spectrometer (PTR-MS)	On-line
Aerosol number (mass) size distribution	Particle	Scanning mobility particle sizer (SMPS, consist of 3081-DMA and 3775-CPC),	On-line
Size resolved non-refractory aerosol	Particle	High resolution time-of-flight aerosol mass spectrometer (HR-ToF-AMS)	On-line

473

474



475 Table 3 Emission factors (EFs) of gaseous pollutants from the gasoline direct injection (GDI) and port fuel injection (PFI) vehicles in
 476 this study and those of previous studies.

	This study				Saliba et al., 2017		May et al., 2014	Platt et al., 2013		Zhu et al., 2016	
	GDI		PFI		GDI	PFI	PFI ^a			GDI	PFI
	China V		China IV		ULEV	ULEV	LEV II	Euro V		China IV	China IV
	Cold BJC				Cold UC ^b		Cold UC	Cold NEDC		Cold WLTC ^c	
	g kg- fuel ⁻¹	g km ⁻¹	g kg- fuel ⁻¹	g km ⁻¹	g km ⁻¹	g km ⁻¹	g kg-fuel ⁻¹	g kg-fuel ⁻¹	g km ⁻¹	g km ⁻¹	g km ⁻¹
CO ₂	3439 ±23	213 ±4	3350 ±24	283 ±4	-	-	-	-	-	187	215
THC	1.55 ±0.22	0.09 ±0.01	1.70 ±0.19	0.13 ±0.01	0.02	0.06	0.64	0.91-1.06	0.036- 0.042	0.05	0.03
Benzene	0.056 ±0.011	0.003 ±0.001	0.061 ±0.016	0.005 ±0.001	-	-	0.018	-	0.002	-	-
Toluene	0.101 ±0.004	0.006 ±0.001	0.220 ±0.047	0.017 ±0.004	-	-	0.026	-	0.002	-	-

477 ^a 22 PFI vehicles and 3 GDI vehicles;

478 ^b UC: Unified Cycle;

479 ^c WLTC: Worldwide-harmonized Light-duty Test Cycle

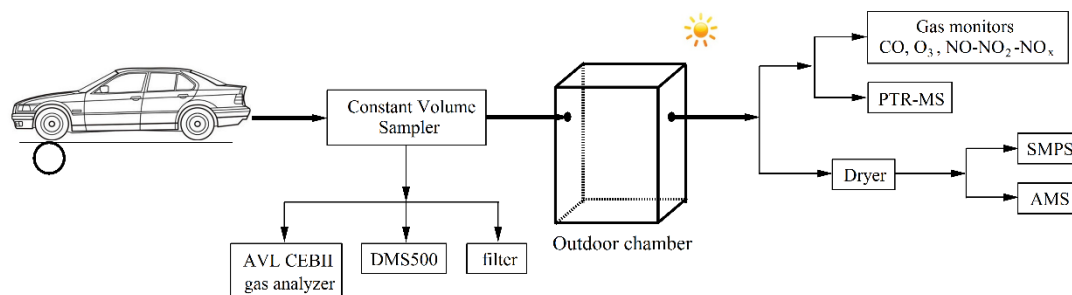


480 Table 4 EFs of primary aerosols, including carbonaceous aerosols and particulate polycyclic aromatic hydrocarbons (PAHs) from the
 481 GDI and PFI vehicles in this study and those of previous studies.

	This study				Saliba et al., 2017		May et al., 2014	Platt et al., 2013		Zhu et al., 2016	
	GDI		PFI		GDI	PFI	PFI			GDI	PFI
	China V		China IV		ULEV	ULEV	LEV II	Euro V		China IV	China IV
	Cold BJC				Cold UC		Cold UC	Cold NEDC		Cold WLTC	
	mg kg- fuel ⁻¹	mg km ⁻¹	mg kg- fuel ⁻¹	mg km ⁻¹	mg km ⁻¹	mg km ⁻¹	mg kg-fuel ⁻¹	mg kg- fuel ⁻¹	mg km ⁻¹	mg km ⁻¹	mg km ⁻¹
PM _{2.5}	61.7±24.5	3.4±1.4	33.4±25.6	2.5±1.9	3.9	2.4	18.0	-	-	1.5	1.0
EC	10.7±3.6	0.6±0.2	2.4±1.6	0.2±0.1	3.0	0.6	12.2	11.2-20.0	1.2-1.7	-	-
POA	41.7±9.8	2.3±0.6	25.0±0.3	1.9±0.1	0.4	0.6	5.2	24.5-19.7	0.4-1.4	-	-
OC/EC	3.2		8.7		0.1	0.8	0.4	0.2-1.8		-	-
PAHs(×10 ⁶)	20.5±2.1	1.1±0.1	13.2±4.1	1.0±0.3	-	-	-	-	-	-	-

482

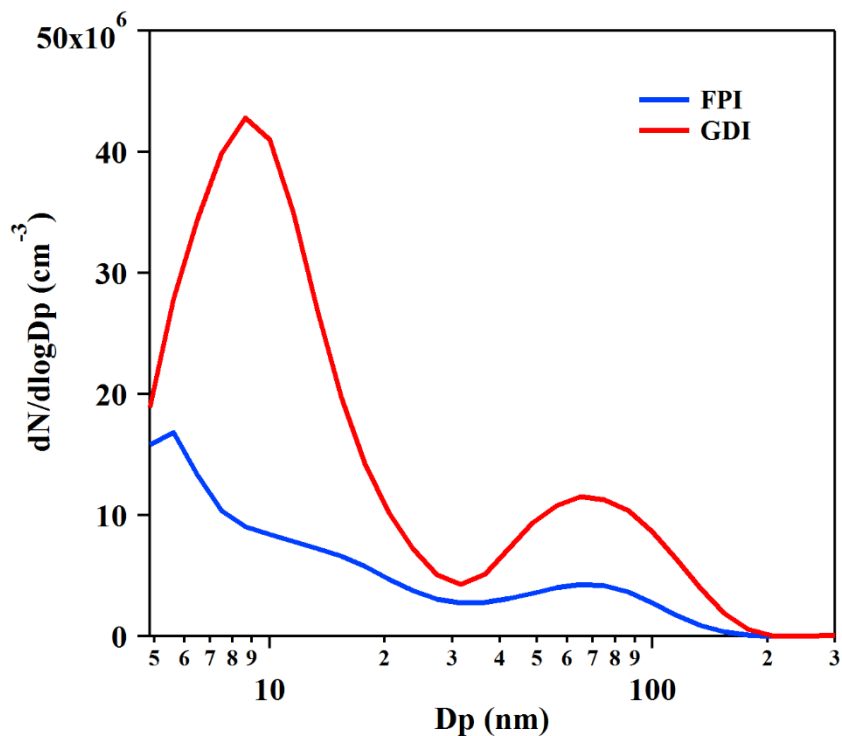
483



484

485 Figure 1. Schematic diagram of the outdoor chamber set up for the experiments.

486

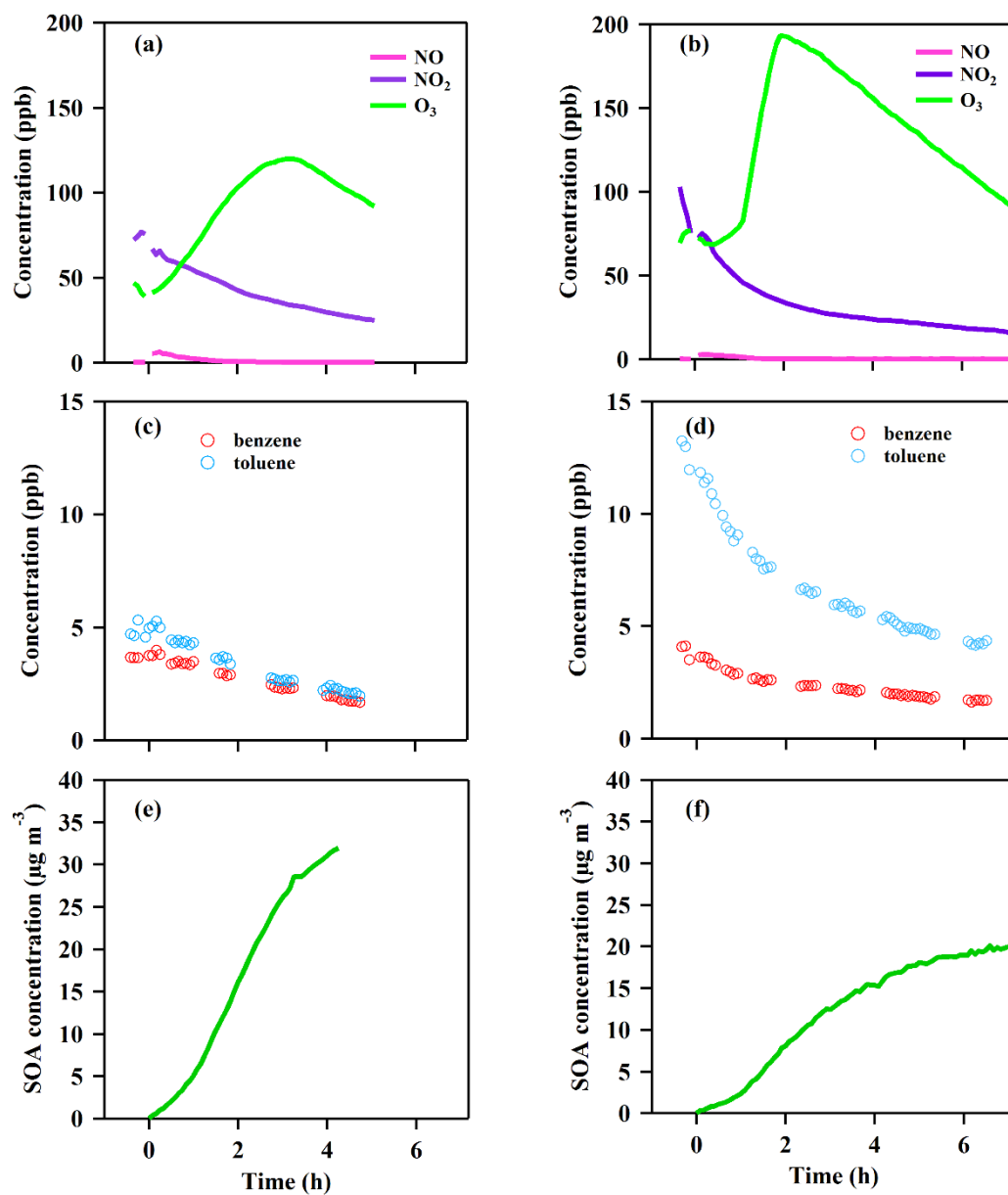


487

488 Figure 2. Number size distributions of primary PM emitted from the GDI (red line) and PFI (blue line) gasoline

489 vehicles.

490



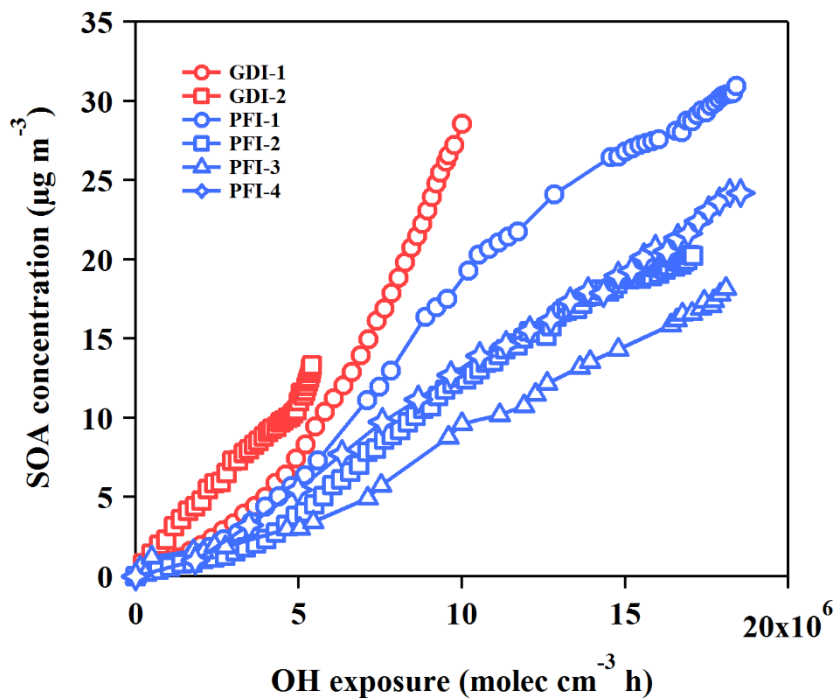
491

492 Figure 3. Time series of the gases and particle evolutions over the photochemical age in the chamber experiments

493 from the GDI vehicle exhaust (a, c, e) and PFI vehicle exhaust (b, d, f). (a, b): NO, NO₂ and O₃ concentration; (c,

494 d): benzene and toluene concentration; (e, f): corrected SOA concentration.

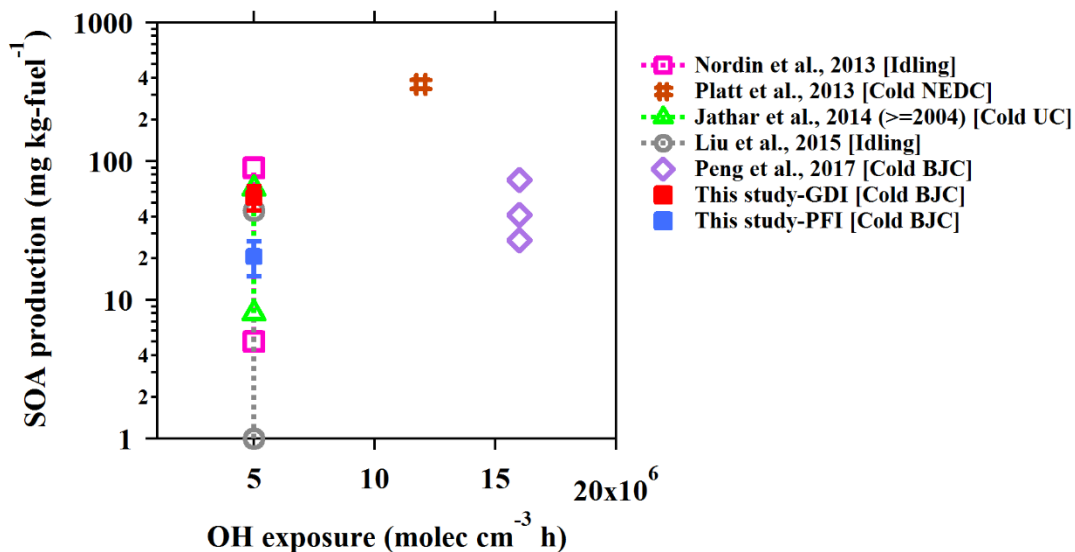
495



496

497 Figure 4. SOA productions from the GDI vehicle exhaust (red markers) and the PFI vehicle exhaust (blue markers)
498 as functions of OH exposure in the chamber experiments.

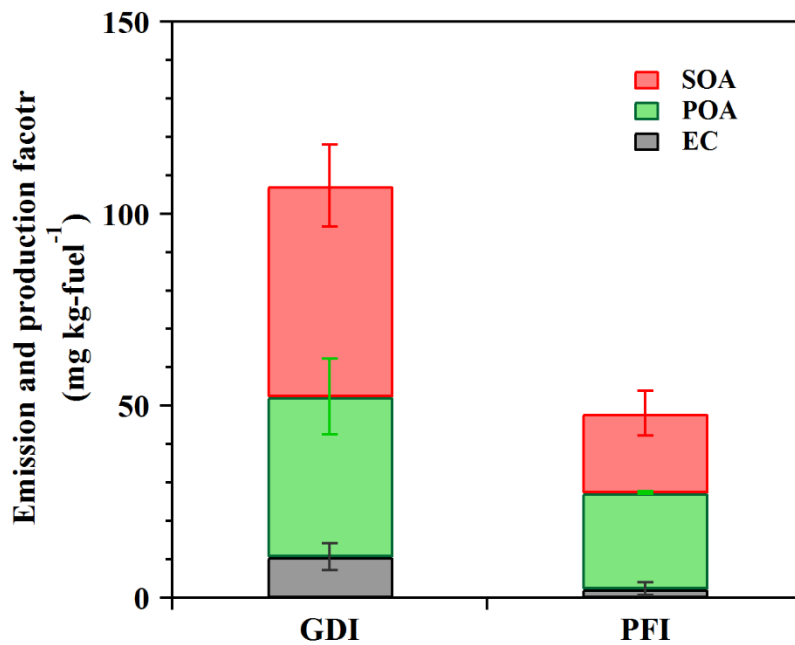
499



500

501 Figure 5. Fuel-based SOA production as a function of OH exposure in the chamber. The SOA production data are
502 from published studies of chamber simulation of gasoline vehicle exhaust. From the study of Jathar et al. (2014),
503 the SOA production of vehicles manufactured in 2004 or later is selected, which is a model year that is more close
504 to those of the vehicles in this study. The driving cycles are also noted in the legend of each study.

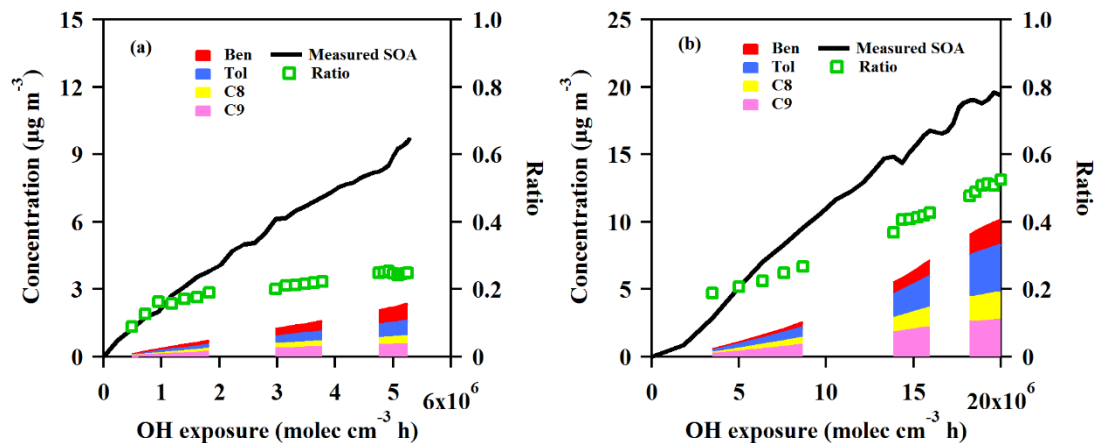
505



506

507 Figure 6 EC and POA EFs as well as corrected SOA production factors from the GDI and PFI vehicle exhausts in
508 this study (OH exposure = 5×10^6 molecular cm^{-3} h).

509



510

511 Figure 7. Measured and predicted SOA concentration as a function of OH exposure from GDI vehicle exhaust (a)
512 and PFI vehicle exhaust (b) in the chamber experiments. The black line is the measured SOA concentration with
513 wall-loss and particle dilution correction during the experiment. The red, blue, yellow and pink areas are predicted
514 SOA concentration estimated from benzene, toluene, C8 benzene and C9 benzene, respectively. The green markers
515 are the ratios of the predicted SOA to the measured SOA.

516